Title

Opto-mechanical characterization of sclera by polarization sensitive optical coherence tomography.

Authors

Shin, Andrew
Park, Joseph
Demer, Joseph

Publication Date

2018-04-27

DOI

10.1016/j.jbiomech.2018.03.017

Peer reviewed

HHS Public Access

Author manuscript

J Biomech. Author manuscript; available in PMC 2019 April 27.

Published in final edited form as:

J Biomech. 2018 April 27; 72: 173–179. doi:10.1016/j.jbiomech.2018.03.017.

Opto-mechanical characterization of sclera by polarization sensitive optical coherence tomography

Andrew Shin[a,f], **Joseph Park**[a,b], and **Joseph L. Demer**[a,c,d,e,*]

[a]Department of Ophthalmology, Stein Eye Institute, University of California, Los Angeles, United States

[b]Department of Bioengineering, University of California, Los Angeles, United States

[c]Biomedical Engineering Interdepartmental Program, University of California, Los Angeles, United States

[d]Neuroscience Interdepartmental Program, University of California, Los Angeles, United States

[e]Department of Neurology, University of California, Los Angeles, United States

[f]Wellman Center for Photomedicine, Harvard Medical School & Massachusetts General Hospital, Boston, United States

Abstract

Polarization sensitive optical coherence tomography (PSOCT) is an interferometric technique sensitive to birefringence. Since mechanical loading alters the orientation of birefringent collagen fibrils, we asked if PSOCT can be used to measure local mechanical properties of sclera.

Infrared (1300 nm) PSOCT was performed during uniaxial tensile loading of fresh scleral specimens of rabbits, cows, and humans from limbal, equatorial, and peripapillary regions. Specimens from 8 human eyes were obtained. Specimens were stretched to failure at 0.01 mm/s constant rate under physiological conditions of temperature and humidity while birefringence was computed every 117 ms from cross-sectional PSOCT. Birefringence modulus (BM) was defined as the rate of birefringence change with strain, and tensile modulus (TM) as the rate of stress change between 0 and 9% strain.

In cow and rabbit, BM and TM were positively correlated with slopes of 0.17 and 0.10 GPa, and with correlation coefficients 0.63 and 0.64 ($P < 0.05$), respectively, following stress-optic coefficients 4.69, and 4.20 GPa^{-1}. In human sclera, BM and TM were also positively correlated with slopes of 0.24 GPa for the limbal, 0.26 GPa for the equatorial, and 0.31 GPa for the peripapillary regions. Pearson correlation coefficients were significant at 0.51, 0.58, and 0.69 for each region, respectively (<0.001). Mean BM decreased proportionately to TM from the limbal to equatorial to peripapillary regions, as stress-optic coefficients were estimated as 2.19, 2.42, and 4.59 GPa^{-1}, respectively.

*Corresponding author at: Stein Eye Institute, 100 Stein Plaza, UCLA, Los Angeles, CA 90095-7002, United States. jld@jsei.ucla.edu (J.L. Demer).

Conflict of interest

None of the authors has any financial or personal relationship that could inappropriately influence this work.

Since birefringence and tensile elastic moduli correlate differently in cow, rabbit, and various regions of human sclera, it might be possible to mechanically characterize the sclera *in vivo* using PSOCT.

Keywords

Birefringence; Optical coherence tomography; Sclera

1. Introduction

Biomechanical properties of various ocular tissues have been reported, including extraocular muscles (EOM) (Quaia et al., 2009; Shin et al., 2015; Yoo et al., 2009), orbital connective tissue and fat (Chen and Weiland, 2011; Schoemaker et al., 2006; Yoo et al., 2011a), cornea (Yoo et al., 2011b), and sclera (Yoo et al., 2011c), with sclera most widely investigated because of its putative role in myopia (McBrien and Gentle, 2003) and glaucoma (Burgoyne et al., 2005). Myopic scleras exhibit abnormally low stiffness and increased creep (McBrien et al., 2009; Phillips et al., 2000), related to structural changes in collagen fiber bundles including lamellar arrangement and fibril diameter (Curtin et al., 1979), associated with extracellular matrix remodeling (McBrien et al., 2009; Summers Rada et al., 2006). Expanded experimental studies has been performed using human sclera collagen cross-linking for myopia treatment (Wang et al., 2012; Wollensak and Spoerl, 2004). Several studies have reported the nonlinear viscoelastic characterization of peripapillary sclera in normal and glaucomatous eyes (Downs et al., 2003; Downs et al., 2005) and biomechanical effect of intraocular pressure (IOP) variations had been investigated both experimentally (Fazio et al., 2012; Girard et al., 2009; Nguyen and Ethier, 2015) and by simulation (Sigal and Ethier, 2009; Sigal et al., 2004). However, the foregoing experiments have required post-mortem methods.

Elastography is a noninvasive imaging method mapping the elastic properties of soft tissues *in vivo* (Ophir et al., 1991), and can be used for diagnosing pathological changes such as edema, fibrosis, or calcification (Gambichler et al., 2005). Ultrasound and magnetic resonance imaging (MRI) are widely used for imaging strain in nearly entire organs (Sarvazyan et al., 2011). However, imaging resolution is limited 30–70 μm for ultrasound (Foster et al., 2000) and 120 μm for MRI (Thali et al., 2004). An alternative method, optical coherence tomography (OCT), has superior spatial resolution of only a few microns, enabling precision OCT elastography to measure the stiffness change after corneal cross linking (Li et al., 2014), and map optic nerve head strain under IOP loading (Girard et al., 2016).

Polarization sensitive OCT (PSOCT) extends conventional OCT by adding polarimetry to provide birefringence information (de Boer et al., 1997). Birefringence is an optical property of anisotropic material whereby its refractive index depends on the polarization and propagation direction of light (Hecht, 2001). Since most biological tissues contain birefringent constituents such as collagen, birefringence imaging has been investigated in ophthalmology (Cense et al., 2004), dermatology (Sakai et al., 2009), and cardiology (Fan

and Yao, 2013). In ophthalmology, anterior (Kasaragod et al., 2016) and posterior (Zotter et al., 2012) ocular imaging has been widely performed to monitor pathological birefringence. PSOCT has been used to measure birefringence and validated to examine collagen organization changes in ex vivo human tissues (Kemp et al., 2005; Kuo et al., 2007; Nadkarni et al., 2007). It is also possible to perform PSOCT elastography, correlating birefringence with mechanical properties (Wiesauer et al., 2005). Correlation has been demonstrated in porcine sclera between birefringence and elastic parameters (Nagase et al., 2013; Yamanari et al., 2012), but this has not been studied in human. Birefringence of human sclera has been correlated with IOP *in vivo* (Yamanari et al., 2014), but direct correlation with mechanical stiffness remains necessary. Therefore, the current study aimed to investigate opto-mechanical correlation in human and other mammalian sclera by capturing concurrent birefringence images during uniaxial tensile loading.

2. Methods

2.1. Specimen preparation

Bovine eyes, aged 20–30 months, were obtained from local abattoir (Manning Beef LLC, Pico Rivera, CA), and New Zealand adult white rabbit (3–4 kg) eyes were obtained by tissue sharing from local research laboratories. Scleral specimens of both cow and rabbit were prepared from the globe equatorial region. Eight human globes of average age 67 ± 16 (standard deviation, SD) years, were obtained from eye banks within three days of death. Globes were wrapped in saline-soaked gauze during overnight shipment to the laboratory. Human specimens were obtained from limbal, equatorial, and peripapillary regions to examine regional differences. Each specimen was trimmed by scalpel to rectangular shape in random orientation (6 ×2 mm including clamping portion) as measured using a digital caliper. An industrial OCT scanner (OCS1300SS, Thorlabs, Inc., Newton, NJ) was used to measure the cross sectional dimensions of scleral specimens. Specimen aspect ratio was 2:1 to avoid artifact (Carew et al., 2003).

2.2. Uniaxial tensile testing with concurrent birefringence measurement

A horizontally mounted micro-tensile load cell was constructed using heavy metallic hardware, a high speed linear motor (Ibex Engineering, Newberry Park, CA), and strain gauge permitting specimen testing in a physiological environment as described elsewhere (Fig. 1) (Shin et al., 2013). Specimens were anchored in a custom milled clamp having serrated surfaces to prevent slip. Specimens were immersed in Ringer's lactate solution before clamping, and continuously kept moisturized in the tensile chamber by high humidity water vapor at physiological temperature under feedback control by a thermocouple adjacent the specimen. Specimens were pre-loaded by 0.05 N to avoid slack, and elongated at constant rate of 0.01 mm/s until failure, as tensile force was recorded by a strain gauge (LSB200, FUTEK Advanced Sensor Technology, Inc., Irvine). Specimens in each region were assumed isotropic. During tensile testing, birefringence was imaged in cross sections using a polarization-sensitive OCT scanner (PSOCT-1300SS, Thorlabs Inc., Newton, NJ). This system incorporates fiber-based Michelson interferometry with polarized beam splitters to calculate birefringence images at 1300 nm with 12 μm axial and 25 μm transverse resolution. Images can be obtained over a 10 mm field at up to 3 mm depth, as limited by

light attenuation. The imaging probe was mounted above the specimen (Fig. 1) so that time sequential, two-dimensional phase retardation images could be obtained every 117 ms as strain was progressively imposed in the tensile load cell. Control experiments were performed with internal sclera surface facing upwards toward the OCT scanner, and vice versa, but no significant difference was found. Since imaging penetration was 3 mm to encompass entire specimen thickness, birefringence measurement was uniform over the entire specimen. Images were processed in spatial domain having signal to noise ratio >5 dB, and temporal domain using a 1.17 s moving average filter. Additional speckle noise reduction algorithm was applied (MATLAB R2016a, The MathWorks, Inc., Natick, MA). Filtered phase retardation values were converted to birefringence Δn using the equation (Hecht, 2001):

$$\Delta n = \frac{\lambda_0}{2\pi L}\Gamma \quad (1)$$

where λ_0 is vacuum wavelength of light source, L is pixel resolution, and, Γ is phase retardation, respectively. Birefringence was measured in range of 0–9% strain regarded as physiological for these ocular tissues (Scarcelli et al., 2012; Wang et al., 2012; Wollensak and Spoerl, 2004), consistent with present findings that many specimens fail at 20% strain or even less. Accordingly, tensile modulus (TM) was calculated as mean slope of the stress-strain curve from 0 to 9% strain.

2.3. Avoiding cancellation by opposite local initial phase

In each cross sectional image pixel, retardation varies from 0 to π depending on initial birefringence state caused by varying alignment of collagen fibers. Since phase retardation increases or decreases with strain in sinusoidal fashion from 0 to π radians, the direction of change in local phase retardation depends upon local starting phase (Fig. 2), although physiological strain would never be great enough to demonstrate sinusoidal periodicity over multiple cycles of retardation. Over small angles, the rate of birefringence change with strain would be approximately linear. Therefore, change in birefringence cannot be determined by averaging the total value over the entire specimen cross section, because phase cancellation would occur due to variations in local starting phase. A practical approach is to confine analysis to regions having similar starting phase retardation values. In this study images were divided into 16 small regions to avoid the cancellation artifact. Since entire sclera specimen was clamped and tension was applied through the whole cross section area, we assumed uniform strain distribution within it and within any subregions.

Birefringence change was presumed to reflect altered collagen fiber orientation under load. In order to correlate opto-mechanical properties of sclera, birefringence modulus (BM) was defined as the rate of birefringence change with strain, which is analogous to the tensile modulus (TM), the rate of stress change with strain. We considered the absolute value of this rate, anticipating that its mean value would be systematically reduced by random inclusion of some initial phases with slope values near zero such as region α in Fig. 2. Nevertheless, this situation would occur uniformly often for all test loadings, and so not bias the results. If

BM is correlated with TM, birefringence signal can be used to infer stress. Generally, various different scleral regions exhibited different initial phases. Even though the absolute rate of change in phase with strain might be identical in each region, a simple graph of phase retardation could exhibit positive or negative slope depending upon initial phase, as seen in Fig. 3.

To calculate overall BM over the entire cross-sections, 16 small individual regions with uniform initial phase were analyzed first, then their absolute slope values were averaged in order to avoid cancellation by opposite-signed slopes as indicated below.

$$B = \frac{1}{16}\sum_{i=1}^{16}|b_i| \quad (2)$$

where B, and b_i are BM of total, and local regions, respectively.

2.4. Modified stress-optic law with birefringence and tensile modulus

The stress-optic law (Dally and Riley, 1991) in photoelasticity characterizing the relation between optical phase retardation and mechanical stress is given by the equation:

$$\Gamma = \frac{2\pi t}{\lambda}C(\sigma_1 - \sigma_2) \quad (3)$$

where Γ is induced retardation, t is specimen thickness, and λ is vacuum wavelength, C is stress-optic coefficient, and σ_1 & σ_2 are the first and second principal stresses, respectively. Recognizing that phase retardation can be expressed as birefringence term using Eq. (1), and uniaxial tensile stress was applied to sclera tissue, Eq. (3) can be rearranged as shown in Eq. (4) for uniaxial tension:

$$\Delta n = C \cdot \sigma \quad (4)$$

where Δn is birefringence, and C is stress-optic coefficient, and σ is uniaxial tensile stress, respectively. In the linear regime, Eq. (4) can be divided by strain (ε), and the stress-optic coefficient can be expressed in terms of BM and TM as shown in Eq. (5):

$$\mathrm{C} = \mathrm{BM}/\mathrm{TM} \quad (5)$$

where BM = $\delta\Delta n/\delta\varepsilon$, and TM = $\delta\sigma = \delta\varepsilon$

3. Results

3.1. Correlated birefringence and tensile modulus

For cow and rabbit sclera, simultaneously measured BM and TM pairs were plotted for analysis (Fig. 4), and the Pearson correlation was computed (GraphPad Software, Inc., La Jolla, CA). Both cow and rabbit scleras exhibited statistically significant positive correlation between BM and TM (Table 1). The mean (± SEM) TM of bovine sclera was larger (19.0 ± 2.3 MPa) than for rabbit (13.0 ± 1.0 MPa), while bovine BM was also larger ($83 \pm 8 \times 10^{-3}$ vs $56 \pm 7 \times 10^{-3}$). Corresponding stress-optic coefficients of bovine and rabbit sclera were 4.69 ± 0.44 and 4.20 ± 0.43 GPa^{-1}, which do not significantly differ.

The foregoing procedure was employed for human scleral specimens. For the three different human scleral regions, BM and TM demonstrated moderate to strong positive correlation (Table 2). Mean values of BM and TM were calculated in each region (Fig. 5). In human, TM decreased from 26 ± 1 MPa in the limbal to 18 ± 1 MPa in equatorial, and to 8.3 ± 0.8 MPa in the peripapillary region, as BM also decreased from $54 \pm 3 \times 10^{-3}$ to $39 \pm 2 \times 10^{-3}$, and to $28 \pm 2 \times 10^{-3}$, respectively. Corresponding stress-optic coefficients were 2.19 ± 0.11, 2.42 ± 0.14, and 4.59 ± 0.54 GPa^{-1}, respectively.

3.2. Opto-mechanical behavior of human sclera

Optical birefringence and mechanical stress values were paired for specimens of human sclera at matching values of strain, and are plotted in Fig. 6 to infer strain for three scleral regions. Fig. 6 illustrates the opto-mechanical behavior of each human scleral region with linear regression relating birefringence with stress. The peripapillary region (0.38 GPa) exhibited different opto-mechanical behavior from limbal and equatorial regions (0.48, and 0.45 GPa). These slopes may be considered as inverse stress-optic coefficients.

4. Discussion

The current study demonstrates that the rate of birefringence change correlates with the tensile modulus of sclera in humans, cows, and rabbits within the 0–9% range of strain that is physiologic for this relatively rigid ocular tissue. Birefringence (BM) and tensile modulus (TM) are positively correlated, meaning that when the sclera is stiffer, the BM is greater. Moreover, regional variation in BM and TM in human limbal, equatorial, and peripapillary sclera is also correlated (Fig. 5): as sclera stiffness decreases from anterior to posterior, BM decreases accordingly. Stress-optic coefficients calculated from these BM and TM values can be regarded as intrinsic opto-mechanical properties of each tissue. Although these values are computed under linear and isotropic assumptions, the stress-optic coefficients are similar for perilimbal and equatorial sclera at 2.19 GPa^{-1} and 2.42 GPa^{-1} having almost identical opto-mechanical properties that in turn differ significantly from peripapillary sclera at 4.59 GPa^{-1}. Unlike the other regions, the narrow peripapillary scleral ring immediately adjacent to the optic nerve has anisotropic circumferential collagen fiber direction as demonstrated by non-linear microscopy (Pijanka et al., 2012; Winkler et al., 2010), small-angle light scattering (Danford et al., 2013; Girard et al., 2011), and wide-angle X-ray scattering (Pijanka et al., 2013; Pijanka et al., 2015). Peripheral to the circumferential scleral ring,

scleral fibers have a wide range of criss-crossing orientations likely to result in grossly isotropic tensile properties. Since the current study did not include the peripapillary ring tissue, which is too small to be loaded outside the clamps in the current experiment, the current assumption of tissue isotropy remains initially reasonable. Since the current study performed uniaxial tensile testing in arbitrary directions that would not have detected possible tissue anisotropy, further study would be required to detect possible anisotropy relative to circumferential and radial directions. Elevation of IOP in whole or half globes might be performed to study birefringence under loading condition, although interpretation of such a study would probably require assumptions about uniformity and isotropy of scleral thickness and mechanical properties.

Recently, an MRI study demonstrated that the nerve and its sheath become taut during adduction eye movement (Demer, 2016). An OCT study showed that significant deformation occurred in temporal optic nerve head region during adduction, but not abduction (Chang et al., 2017). The current opto-mechanical correlation study could be applied to extend these *in vivo* studies by providing inferred peripapillary stress from OCT birefringence measurement, providing intrinsic mechanical characterization for individual tissues. Since the current study employed an industrial PSOCT scanner and not a clinically approved instrument, further development would be necessary for studies in living humans. Currently, OCT is extensively utilized in ophthalmology to diagnose glaucoma and retinal disorders by structural analysis. (Mwanza et al., 2011; Sung et al., 2012). There already exist clinical OCT scanners that are polarization-sensitive, and used to diagnose pathologic tissues from birefringence signal changes in the retinal nerve fiber layer (RNFL) (Zotter et al., 2012), choroid (Pircher et al., 2011), and posterior sclera (Sugiyama et al., 2015). Since the current study characterized the birefringence-stress relation in human peripapillary sclera, this correlation might be directly applied *in vivo* using clinical PSOCT to infer peripapillary stress both in normal and abnormal sclera tissues.

Once the stress-optic coefficient of a tissue is established in normal subjects, it could be used as a reference for abnormality. Direct correlation between scleral birefringence and stress might be utilized for *in vivo* diagnosis of tissue abnormality, and local anatomic correlation. One possible application might be the longitudinal, *in vivo* study of peripapillary atrophy that frequently occurs on the temporal side (Jonas et al., 1989) and that has been proposed to be due to local strain resulting from optic nerve sheath tethering during adduction eye rotation (Demer, 2016). Peripapillary atrophy frequently occurs with glaucoma (Jonas et al., 2004; Xu et al., 2007), and is progressive with age (Savatovsky et al., 2015), myopia (Nakazawa et al., 2008), and glaucoma progression (Budde and Jonas, 2004; Rockwood and Anderson, 1988; Uchida et al., 1998; Uhm et al., 1998), yet its causation and potential clinical significance remain obscure. If birefringence change were found to be spatially correlated with existing and especially progressing peripapillary atrophy on longitudinal study, this might suggest a causative relationship.

The current study is subject to some limitations. First, even analysis of 16 local regions of each OCT cross section to minimize initial phase cancellation effects may nevertheless have permitted some since the local regions are still large relative to individual collagen fiber bundles. Even finer local analysis might further reduce phase cancellation effects. Additional

factors besides mechanical loading might affect birefringence, including structural (Malik et al., 1992) or composition (Rada et al., 2000) changes in sclera tissue associated with aging. Those changes substantially alter scleral stiffness (Geraghty et al., 2012; Grytz et al., 2014), but might also differently affect birefringence. Specific studies of possible aging effects are probably warranted. The current technique avoided experimental artifact that might have arisen from variation in tissue hydration during testing. The 0–9% strain range employed here is low compared with physiologic strains experienced by, for example, skin or aortic wall; however, since ocular dimensions must remain highly precise to enable adequate visual performance, it is understandable that the ocular sclera does not experience substantially higher strains than about 10% under physiological conditions. A recent study with terahertz (THz) spectroscopy reported that differences in water content influence the accuracy of calculated optical properties since THz radiation is strongly absorbed by water (Png et al., 2008). To avoid the possibility that variations in scleral water content might similarly influence birefringence, we studied fresh tissue under physiological conditions with regulated tissue hydration and temperature throughout each loading, eliminating hydration variation a confounding factor.

Acknowledgments

Supported by U.S. Public Health Service, National Eye Institute: grants EY008313 and EY000331, and Unrestricted Grant from Research to Blindness. The funding sources had no involvement in the design or interpretation of the study, nor in the writing of this paper. No other authors contributed to the writing of this paper. J. Demer is Arthur L. Rosenbaum Professor of Pediatric Ophthalmology.

References

Budde WM, Jonas JB. Enlargement of parapapillary atrophy in follow-up of chronic open-angle glaucoma. Am J Ophthalmol. 2004; 137:646–654. [PubMed: 15059703]

Burgoyne CF, Crawford Downs J, Bellezza AJ, Francis Suh JK, Hart RT. The optic nerve head as a biomechanical structure: a new paradigm for understanding the role of IOP-related stress and strain in the pathophysiology of glaucomatous optic nerve head damage. Prog Retin Eye Res. 2005; 24:39–73. [PubMed: 15555526]

Carew EO, Patel J, Garg A, Houghtaling P, Blackstone E, Vesely I. Effect of specimen size and aspect ratio on the tensile properties of porcine aortic valve tissues. Ann Biomed Eng. 2003; 31:526–535. [PubMed: 12757197]

Cense B, Chen TC, Park BH, Pierce MC, de Boer JF. Thickness and birefringence of healthy retinal nerve fiber layer tissue measured with polarization-sensitive optical coherence tomography. Invest Ophthalmol Vis Sci. 2004; 45:2606–2612. [PubMed: 15277483]

Chang MY, Shin A, Park J, Nagiel A, Lalane RA, Schwartz SD, Demer JL. Deformation of optic nerve head and peripapillary tissues by horizontal duction. Am J Ophthalmol. 2017; 174:85–94. [PubMed: 27751810]

Chen K, Weiland JD. Mechanical properties of orbital fat and its encapsulating connective tissue. J Biomech Eng. 2011; 133:064505. [PubMed: 21744934]

Curtin BJ, Iwamoto T, Renaldo DP. Normal and staphylomatous sclera of high myopia: an electron microscopic study. Arch Ophthalmol. 1979; 97:912–915. [PubMed: 444126]

Dally, JW., Riley, WF. Experimental Stress Analysis. McGraw-Hill Inc; New York: 1991.

Danford FL, Yan D, Dreier RA, Cahir TM, Girkin CA, Vande Geest JP. Differences in the region- and depth-dependent microstructural organization in normal versus glaucomatous human posterior sclerae. Invest Ophthalmol Vis Sci. 2013; 54:7922–7932. [PubMed: 24204041]

de Boer JF, Milner TE, van Gemert MJC, Nelson JS. Two-dimensional birefringence imaging in biological tissue by polarization-sensitive optical coherence tomography. Opt Lett. 1997:22, 934–936. [PubMed: 18183090]

Demer JL. Optic nerve sheath as a novel mechanical load on the globe in ocular duction. Invest Ophthalmol Vis Sci. 2016; 57:1826–1838. [PubMed: 27082297]

Downs JC, Suh JK, Thomas KA, Bellezza AJ, Burgoyne CF, Hart RT. Viscoelastic characterization of peripapillary sclera: material properties by quadrant in rabbit and monkey eyes. J Biomech Eng. 2003; 125:124–131. [PubMed: 12661206]

Downs JC, Suh JK, Thomas KA, Bellezza AJ, Hart RT, Burgoyne CF. Viscoelastic material properties of the peripapillary sclera in normal and early-glaucoma monkey eyes. Invest Ophthalmol Vis Sci. 2005; 46:540–546. [PubMed: 15671280]

Fan C, Yao G. Imaging myocardial fiber orientation using polarization sensitive optical coherence tomography. Biomed Opt Express. 2013; 4:460–465. [PubMed: 23504508]

Fazio MA, Grytz R, Bruno L, Girard MJ, Gardiner S, Girkin CA, Downs JC. Regional variations in mechanical strain in the posterior human sclera. Invest Ophthalmol Vis Sci. 2012; 53:5326–5333. [PubMed: 22700704]

Foster FS, Pavlin CJ, Harasiewicz KA, Christopher DA, Turnbull DH. Advances in ultrasound biomicroscopy. Ultrasound Med Biol. 2000; 26:1–27. [PubMed: 10687788]

Gambichler T, Moussa G, Sand M, Sand D, Altmeyer P, Hoffmann K. Applications of optical coherence tomography in dermatology. J Dermatol Sci. 2005; 40:85–94. [PubMed: 16139481]

Geraghty B, Jones SW, Rama P, Akhtar R, Elsheikh A. Age-related variations in the biomechanical properties of human sclera. J Mech Behav Biomed Mater. 2012; 16:181–191. [PubMed: 23182387]

Girard MJ, Dahlmann-Noor A, Rayapureddi S, Bechara JA, Bertin BM, Jones H, Albon J, Khaw PT, Ethier CR. Quantitative mapping of scleral fiber orientation in normal rat eyes. Invest Ophthalmol Vis Sci. 2011; 52:9684–9693. [PubMed: 22076988]

Girard MJA, Beotra MR, Chin KS, Sandhu A, Clemo M, Nikita E, Kamal DS, Papadopoulos M, Mari JM, Aung T, Strouthidis NG. In vivo 3-dimensional strain mapping of the optic nerve head following intraocular pressure lowering by trabeculectomy. Ophthalmology. 2016; 123:1190–1200. [PubMed: 26992836]

Girard MJA, Suh JKF, Bottlang M, Burgoyne CF, Downs JC. Scleral biomechanics in the aging monkey eye. Invest Ophthalmol Vis Sci. 2009; 50:5226–5237. [PubMed: 19494203]

Grytz R, Fazio MA, Libertiaux V, Bruno L, Gardiner S, Girkin CA, Downs JC. Age- and race-related differences in human scleral material properties. Invest Ophthalmol Vis Sci. 2014; 55:8163–8172. [PubMed: 25389203]

Hecht, E. Optics. Addison-Wesley; 2001.

Jonas JB, Martus P, Horn FK, Junemann A, Korth M, Budde WM. Predictive factors of the optic nerve head for development or progression of glaucomatous visual field loss. Invest Ophthalmol Vis Sci. 2004; 45:2613–2618. [PubMed: 15277484]

Jonas JB, Nguyen XN, Gusek GC, Naumann GO. Parapapillary chorioretinal atrophy in normal and glaucoma eyes. I. Morphometric data. Invest Ophthalmol Vis Sci. 1989; 30:908–918. [PubMed: 2722447]

Kasaragod D, Fukuda S, Ueno Y, Hoshi S, Oshika T, Yasuno Y. Objective evaluation of functionality of filtering bleb based on polarization-sensitive optical coherence tomography. Invest Ophthalmol Vis Sci. 2016; 57:2305–2310. [PubMed: 27127929]

Kemp NJ, Zaatari HN, Park J, Rylander HG Iii, Milner TE. Form-biattenuance in fibrous tissues measured with polarization-sensitive optical coherence tomography (PS-OCT). Opt Express. 2005; 13:4611–4628. [PubMed: 19495377]

Kuo WC, Chou NK, Chou C, Lai CM, Huang HJ, Wang SS, Shyu JJ. Polarization-sensitive optical coherence tomography for imaging human atherosclerosis. Appl Optics. 2007; 46:2520–2527.

Li J, Han Z, Singh M, Twa MD, Larin KV. Differentiating untreated and cross-linked porcine corneas of the same measured stiffness with optical coherence elastography. J Biomed Opt. 2014; 19:110502. [PubMed: 25408955]

Malik NS, Moss SJ, Ahmed N, Furth AJ, Wall RS, Meek KM. Ageing of the human corneal stroma: structural and biochemical changes. Biochim Biophys Acta Mol Basis Dis. 1992; 1138:222–228.

McBrien NA, Gentle A. Role of the sclera in the development and pathological complications of myopia. Prog Retin Eye Res. 2003; 22:307–338. [PubMed: 12852489]

McBrien NA, Jobling AI, Gentle A. Biomechanics of the sclera in myopia: extracellular and cellular factors. Optom Vis Sci. 2009; 86:E23–E30. [PubMed: 19104466]

Mwanza JC, Oakley JD, Budenz DL, Anderson DR. Ability of cirrus HD-OCT optic nerve head parameters to discriminate normal from glaucomatous eyes. Ophthalmology. 2011; 118(241–248):e241.

Nadkarni SK, Pierce MC, Park BH, de Boer JF, Whittaker P, Bouma BE, Bressner JE, Halpern E, Houser SL, Tearney GJ. Measurement of collagen and smooth muscle cell content in atherosclerotic plaques using polarization-sensitive optical coherence tomography. J Am College Cardiol. 2007; 49:1474–1481.

Nagase S, Yamanari M, Tanaka R, Yasui T, Miura M, Iwasaki T, Goto H, Yasuno Y. Anisotropic alteration of scleral birefringence to uniaxial mechanical strain. PLoS One. 2013; 8:e58716. [PubMed: 23536816]

Nakazawa M, Kurotaki J, Ruike H. Longterm findings in peripapillary crescent formation in eyes with mild or moderate myopia. Acta Ophthalmol. 2008; 86:626–629. [PubMed: 18577184]

Nguyen TD, Ethier CR. Biomechanical assessment in models of glaucomatous optic neuropathy. Exp Eye Res. 2015; 141:125–138. [PubMed: 26115620]

Ophir J, Céspedes I, Ponnekanti H, Yazdi Y, Li X. Elastography: a quantitative method for imaging the elasticity of biological tissues. Ultrasonic Imaging. 1991; 13:111–134. [PubMed: 1858217]

Phillips JR, Khalaj M, McBrien NA. Induced myopia associated with increased scleral creep in chick and tree shrew eyes. Invest Ophthalmol Vis Sci. 2000; 41:2028–2034. [PubMed: 10892839]

Pijanka JK, Abass A, Sorensen T, Elsheikh A, Boote C. A wide-angle X-ray fibre diffraction method for quantifying collagen orientation across large tissue areas: application to the human eyeball coat. J Appl Crystallogr. 2013; 46:1481–1489.

Pijanka JK, Coudrillier B, Ziegler K, Sorensen T, Meek KM, Nguyen TD, Quigley HA, Boote C. Quantitative mapping of collagen fiber orientation in non-glaucoma and glaucoma posterior human sclerae. Invest Ophthalmol Vis Sci. 2012; 53:5258–5270. [PubMed: 22786908]

Pijanka JK, Spang MT, Sorensen T, Liu J, Nguyen TD, Quigley HA, Boote C. Depth-dependent changes in collagen organization in the human peripapillary sclera. PLoS One. 2015; 10:e0118648. [PubMed: 25714753]

Pircher M, Hitzenberger CK, Schmidt-Erfurth U. Polarization sensitive optical coherence tomography in the human eye. Prog Retin Eye Res. 2011; 30:431–451. [PubMed: 21729763]

Png GM, Choi JW, Ng BW, Mickan SP, Abbott D, Zhang XC. The impact of hydration changes in fresh bio-tissue on THz spectroscopic measurements. Phys Med Biol. 2008; 53:3501–3517. [PubMed: 18552421]

Quaia C, Ying HS, Optican LM. The viscoelastic properties of passive eye muscle in primates. II: testing the quasi-linear theory. PLoS One. 2009; 4:e6480. [PubMed: 19649257]

Rada JA, Achen VR, Penugonda S, Schmidt RW, Mount BA. Proteoglycan composition in the human sclera during growth and aging. Invest Ophthalmol Vis Sci. 2000; 41:1639–1648. [PubMed: 10845580]

Rockwood EJ, Anderson DR. Acquired peripapillary changes and progression in glaucoma. Graefes Arch Clin Exp Ophthalmol. 1988; 226:510–515. [PubMed: 3209077]

Sakai S, Nakagawa N, Yamanari M, Miyazawa A, Yasuno Y, Matsumoto M. Relationship between dermal birefringence and the skin surface roughness of photoaged human skin. J Biomed Opt. 2009; 14:044032–044032 044038. [PubMed: 19725743]

Sarvazyan A, Hall TJ, Urban MW, Fatemi M, Aglyamov SR, Garra BS. An overview of elastography – an emerging branch of medical imaging. Curr Med Imaging Rev. 2011; 7:255–282. [PubMed: 22308105]

Savatovsky E, Mwanza JC, Budenz DL, Feuer WJ, Vandenbroucke R, Schiffman JC, Anderson DR, Ocular Hypertension Treatment, S. Longitudinal changes in peripapillary atrophy in the ocular

hypertension treatment study: a case-control assessment. Ophthalmology. 2015; 122:79–86. [PubMed: 25208858]

Scarcelli G, Pineda R, Yun SH. Brillouin optical microscopy for corneal biomechanics. Invest Ophthalmol Visual Sci. 2012; 53:185–190. [PubMed: 22159012]

Schoemaker I, Hoefnagel PP, Mastenbroek TJ, Kolff CF, Schutte S, van der Helm FC, Picken SJ, Gerritsen AF, Wielopolski PA, Spekreijse H, Simonsz HJ. Elasticity, viscosity, and deformation of orbital fat. Invest Ophthalmol Vis Sci. 2006; 47:4819–4826. [PubMed: 17065493]

Shin A, Yoo L, Demer JL. Biomechanics of superior oblique Z-tenotomy. J AAPOS. 2013; 17:612–617. [PubMed: 24321425]

Shin A, Yoo L, Demer JL. Independent active contraction of extraocular muscle compartments. Invest Ophthalmol Vis Sci. 2015; 56:199–206.

Sigal IA, Ethier CR. Biomechanics of the optic nerve head. Exp Eye Res. 2009; 88:799–807. [PubMed: 19217902]

Sigal IA, Flanagan JG, Tertinegg I, Ethier CR. Finite element modeling of optic nerve head biomechanics. Invest Ophthalmol Vis Sci. 2004; 45:4378–4387. [PubMed: 15557446]

Sugiyama S, Hong YJ, Kasaragod D, Makita S, Uematsu S, Ikuno Y, Miura M, Yasuno Y. Birefringence imaging of posterior eye by multi-functional Jones matrix optical coherence tomography. Biomed Opt Express. 2015; 6:4951–4974. [PubMed: 26713208]

Summers Rada JA, Shelton S, Norton TT. The sclera and myopia. Exp Eye Res. 2006; 82:185–200. [PubMed: 16202407]

Sung KR, Wollstein G, Kim NR, Na JH, Nevins JE, Kim CY, Schuman JS. Macula assessment using optical coherence tomography for glaucoma diagnosis. Br J Ophthalmol. 2012; 96:1452–1455. [PubMed: 23018425]

Thali MJ, Dirnhofer R, Becker R, Oliver W, Potter K. Is ‘virtual histology’ the next step after the ‘virtual autopsy’? Magnetic resonance microscopy in forensic medicine. Magn Reson Imaging. 2004; 22:1131–1138. [PubMed: 15528000]

Uchida H, Ugurlu S, Caprioli J. Increasing peripapillary atrophy is associated with progressive glaucoma. Ophthalmology. 1998; 105:1541–1545. [PubMed: 9709771]

Uhm KB, Lee DY, Kim JT, Hong C. Peripapillary atrophy in normal and primary open-angle glaucoma. Korean J Ophthalmol. 1998; 12:37–50. [PubMed: 9753950]

Wang M, Zhang F, Qian X, Zhao X. Regional biomechanical properties of human sclera after cross-linking by riboflavin/ultraviolet A. J Refract Surg. 2012; 28:723–728. [PubMed: 23062003]

Wiesauer K, Dufau ADS, Götzinger E, Pircher M, Hitzenberger CK, Stifter D. Non-destructive quantification of internal stress in polymer materials by polarisation sensitive optical coherence tomography. Acta Mater. 2005; 53:2785–2791.

Winkler M, Jester B, Nien-Shy C, Massei S, Minckler DS, Jester JV, Brown DJ. High resolution three-dimensional reconstruction of the collagenous matrix of the human optic nerve head. Brain Res Bull. 2010; 81:339–348. [PubMed: 19524027]

Wollensak G, Spoerl E. Collagen crosslinking of human and porcine sclera. J Cataract Refract Surgery. 2004; 30:689–695.

Xu L, Wang Y, Yang H, Jonas JB. Differences in parapapillary atrophy between glaucomatous and normal eyes: the Beijing Eye Study. Am J Ophthalmol. 2007; 144:541–546. [PubMed: 17651676]

Yamanari M, Ishii K, Fukuda S, Lim Y, Duan L, Makita S, Miura M, Oshika T, Yasuno Y. Optical rheology of porcine sclera by birefringence imaging. PLoS One. 2012; 7:e44026. [PubMed: 22970158]

Yamanari M, Nagase S, Fukuda S, Ishii K, Tanaka R, Yasui T, Oshika T, Miura M, Yasuno Y. Scleral birefringence as measured by polarization-sensitive optical coherence tomography and ocular biometric parameters of human eyes in vivo. Biomed Opt Express. 2014; 5:1391–1402. [PubMed: 24877003]

Yoo L, Gupta V, Lee C, Kavehpore P, Demer JL. Viscoelastic properties of bovine orbital connective tissue and fat: constitutive models. Biomech Model Mechanobiol. 2011a; 10:901–914. [PubMed: 21207094]

Yoo L, Kim H, Gupta V, Demer JL. Quasilinear viscoelastic behavior of bovine extraocular muscle tissue. Invest Ophthalmol Vis Sci. 2009; 50:3721–3728. [PubMed: 19357357]

Yoo L, Reed J, Gimzewski JK, Demer JL. Mechanical interferometry imaging for creep modeling of the cornea. Invest Ophthalmol Vis Sci. 2011b; 52:8420–8424. [PubMed: 21969299]

Yoo L, Reed J, Shin A, Kung J, Gimzewski JK, Poukens V, Goldberg RA, Mancini R, Taban M, Moy R, Demer JL. Characterization of ocular tissues using micro-indentation and Hertzian viscoelastic models. Invest Ophthalmol Vis Sci. 2011c; 52:3475–3482. [PubMed: 21310907]

Zotter S, Pircher M, Torzicky T, Baumann B, Yoshida H, Hirose F, Roberts P, Ritter M, Schütze C, Götzinger E, Trasischker W, Vass C, Schmidt-Erfurth U, Hitzenberger CK. Large-field high-speed polarization sensitive spectral domain OCT and its applications in ophthalmology. Biomed Opt Express. 2012; 3:2720–2732. [PubMed: 23162711]

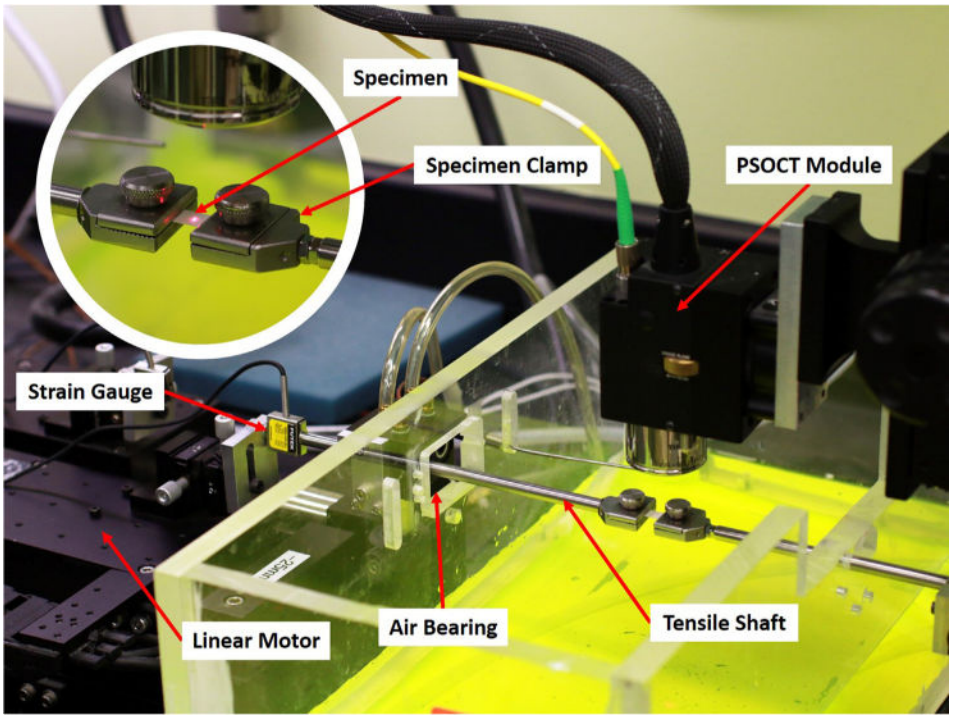

Fig. 1.

Tensile load cell equipped for PSOCT. A linear motor at left connected to a strain gauge transmitted tensile force through a cylindrical shaft supported by frictionless air bearing to the moveable specimen clamp. The other specimen clamp at right was anchored at right. The chamber surrounding the specimen was maintained at physiologic temperature and saturated humidity by heated water (dyed yellow for visibility). The infrared PSOCT camera mounted above the specimen was aimed using a visible red guide laser here illuminating a paper target for illustrative purposes (inset). Actual specimen dimensions were 4 × 2 mm between the clamps. (For interpretation of the references to colour in this figure legend, the reader is referred to the web version of this article.)

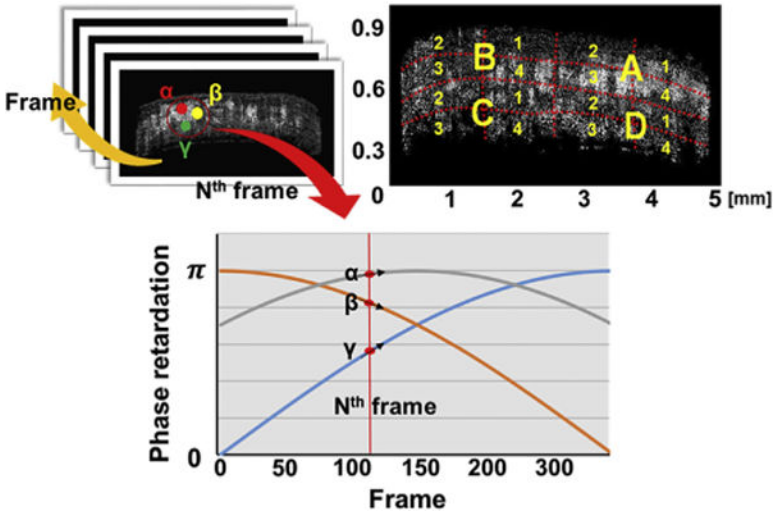

Fig. 2.

Avoiding cancellation due to variations in initial phase retardation. Sequential two-dimensional phase retardation images were obtained at N^{th} frame. Local regions α, β and γ have different directions of changes in birefringence causing cancellation if their birefringence moduli (BM) are simply summed through the entire specimen cross section. To minimize cancellation, each cross section was divided into 16 regions (A1 to D4), and BM was computed for each region. There was little variation in initial phase within each of the 16 regions. Surface reflection has been removed from the Oct images.

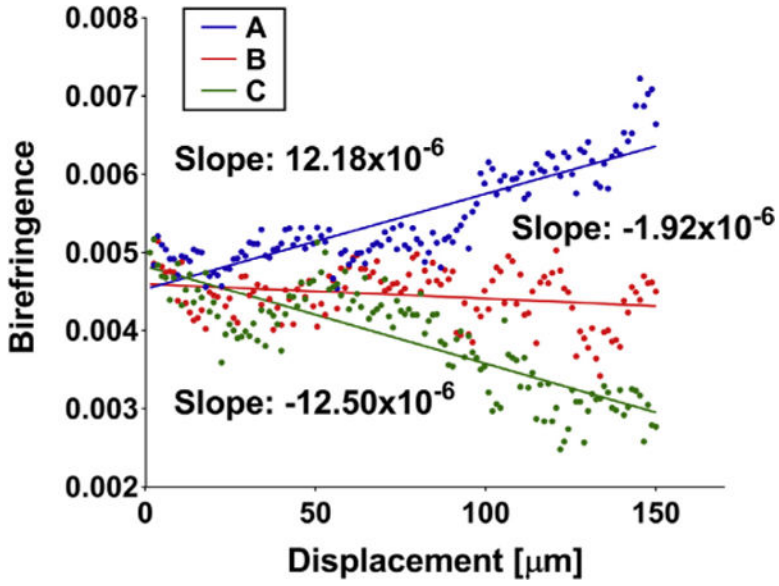

Fig. 3.

Different birefringence behavior of three local regions of the bovine sclera. Although regions A and C showed similar absolute birefringence changes, simple summation could result in the cancellation because of the opposite signed slopes. Each local birefringence series was shifted to start at 0.005 for comparison.

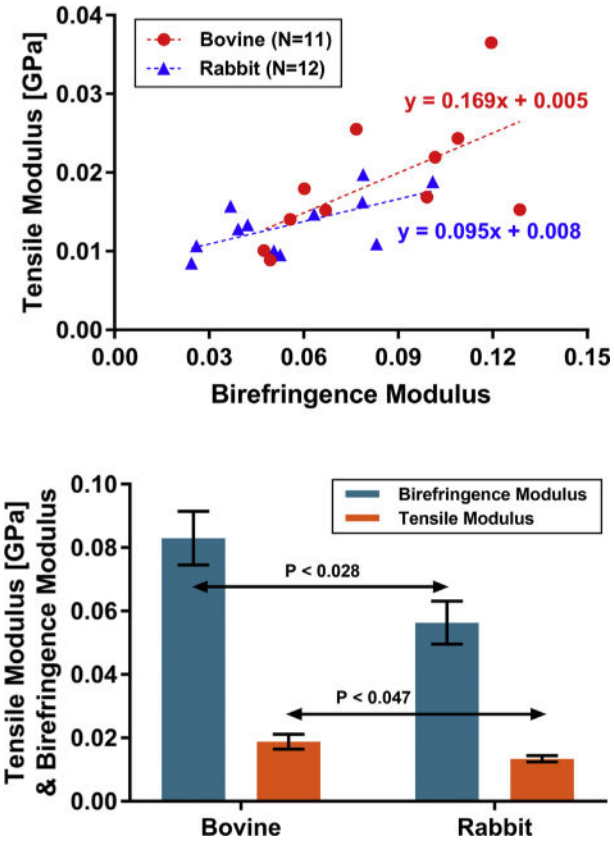

Fig. 4.

Correlation between birefringence and tensile modulus in bovine and rabbit sclera. Stress-optic coefficients were 4.69, and 4.20 GPa^{-1}, respectively.

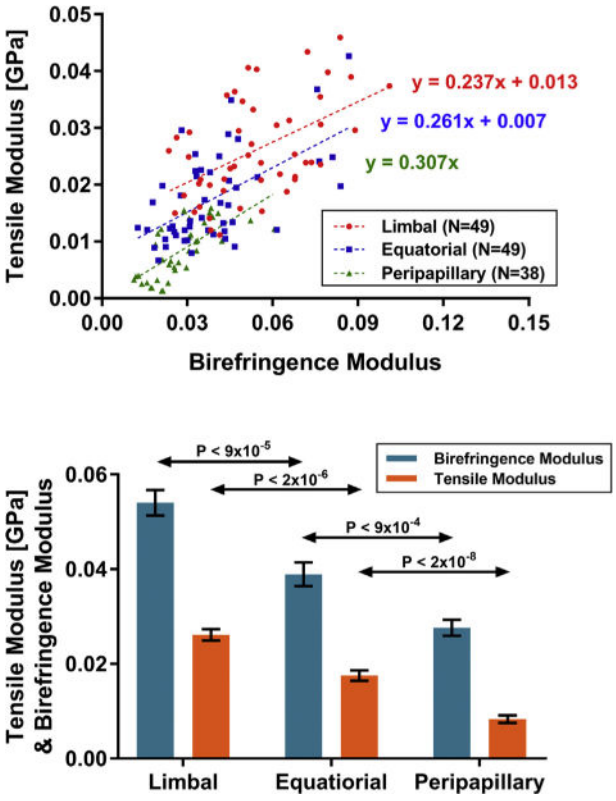

Fig. 5.

Correlation between birefringence and tensile modulus in human sclera. Linear regressions illustrate positive correlation in all three regions, as mean BM and TM progressively decreased from limbal to peripapillary region. Estimated stress-optic coefficients are 2.19, 2.42, and 4.59 GPa^{-1}, respectively.

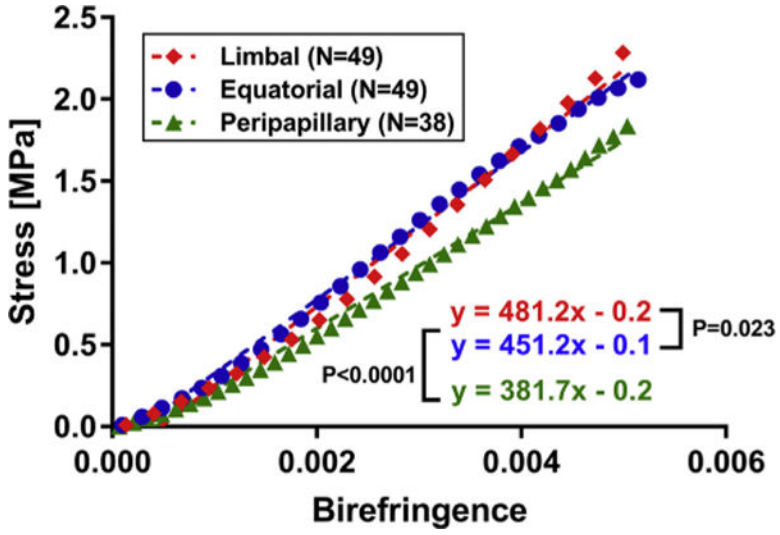

Fig. 6.

Correlation of birefringence and stress in human sclera. Nonlinear stress values were paired with corresponding birefringence values based on matching strain. The slope of the relationship in the peripapillary region (green triangles) is highly significantly different from other two regions ($P < 0.0001$), corresponding to differing inverse stress-optic coefficients. (For interpretation of the references to colour in this figure legend, the reader is referred to the web version of this article.)

Table 1

Correlation between birefringence (BM) and tensile (TM) modulus in bovine and rabbit sclera. Both bovine and rabbit exhibited statically significant positive correlation.

	Bovine	Rabbit
Pearson r	0.6299	0.6346
P value	0.0378	0.0267

Table 2

Correlation between birefringence and tensile modulus in human sclera.

	Limbal	Equatorial	Peripapillary
Pearson r	0.5117	0.5757	0.6943
P value	0.0002	<0.0001	<0.0001